Investigation of pyrite-weathering processes in the vadose zone using optical oxygen sensors

H. Hecht · M. Kölling

Abstract Pyrite weathering in the unsaturated zone of overburden material was investigated in column experiments. Optodes were used to monitor changes in oxygen concentrations. Oxygen recharge in the vadose zone and effects of secondary reactions were investigated. Oxygen transport limits thickness and the rate of the depyritisation. The overburden material (thickness 0.6 m, initial pyrite content 1.2 wt%) was depyritised within 200 days. The position of the pyrite decomposition front, the momentary release of reaction products and the remaining acidification potential can be determined. Buffer capacity, speciation and seepage water velocity are crucial for the distribution of the reaction products and the resulting acidification (minimum pH 1.6). A total of 75% of the protons were consumed by buffering reactions and 15% were fixed to complexes. Only 10% of the protons are represented by the measured pH value. In oxygen-consuming environments optical oxygen measurements can be used to identify and quantify structures and processes.

Keywords Oxygen diffusion · Optode · Pyrite · Vadose zone · Weathering

Introduction

Pyrite decomposition occurs whenever pyrite-bearing sediments are aerated. Such conditions are induced by lowering of the ground water table for open-cast lignite mining and especially by the mining process where large amounts of pyrite-bearing overburden material may become exposed on the dump side of the mines. The result is the formation of acid mine drainage (AMD) by redox reactions that consume oxygen and release large amounts of iron, sulfate and protons. By this process, seepage water with pH values below pH 1 and iron and sulfate concentrations in the range of moles per litre may develop, resulting in dissolution and desorption reactions that are comparable to an acid extraction. Under these conditions, special secondary minerals such as schwertmannite may form.

Pyrite can be oxidised by both oxygen and ferric iron. The oxidation of pyrite can be described as a sequence of different redox processes. Nordstrom (1982) gives an overview of the different partial and sum reactions. In this paper, two equations are the basis for all calculations. Equation (1) describes pyrite decomposition at low pH values that is microbiologically catalysed by *Thiobacillus ferrooxidans*. The reaction rates are limited by either the available pyrite surface or by the oxygen supply depending upon environmental conditions. Equation (1) is the sum reaction of two crucial processes of the pyrite decomposition: the pyrite oxidation by ferric iron and the subsequent oxidation of the evolving ferrous iron with oxygen.

$$FeS_2 + 15/4O_2 + 1/2H_2O \rightarrow Fe^{3+} + 2SO_4^{2-} + H^+ \quad (1)$$

$$FeS_2 + 14Fe^{3+} + 8H_2O \rightarrow 15Fe^{2+} + 2SO_4^{2-} + 16H^+ \quad (2)$$

Equation (2) shows the pyrite oxidation with ferric iron and is of importance if the reaction products of Eq. (1) get into an anoxic pyrite-bearing system. In this case no oxidation of the evolving ferrous iron is observed. The extreme chemistry of acid mine drainage results in extensive secondary reactions. Among them are different buffer reactions (calcite dissolution, silicate decomposition), exchange reactions, formation of complexes, solution and precipitation. A comprehensive overview of pyrite decomposition and subsequent secondary processes is given by Appelo and Postma (1994), Evangelou (1995), Lawson (1982) and Nordstrom (1982).

In the unsaturated zone, different processes are involved in oxygen transport. Diffusion is the major process balancing concentrations in ground air. In seepage water, diffusion is approximately 10,000 times smaller than in ground air, thus being of minor importance. Fick's laws describe the diffusion-driven movement of gaseous

Received: 17 December 2001 / Accepted: 26 March 2002
Published online: 15 May 2002

H. Hecht · M. Kölling (✉)
University of Bremen, Department of Geosciences,
Klagenfurther Str., 28359 Bremen, Germany
E-mail: koelling@uni-bremen.de
Tel.: +49-421-2183928
Fax: +49-421-2184321

 DOI 10.1007/s00254-002-0583-2

molecules. The convective movement of the gaseous phase can be affected by different mechanisms that result in variations of volume or pressure in soil air. Overall, the fraction of convective gas exchange within the soil and between soil air and atmosphere is well below 10% in natural systems (Mattheß 1991). In most systems affected by pyrite decomposition, the transport of dissolved oxygen within the seepage water only plays a subordinated role because of its low solubility. The movement of water in the unsaturated zone is based mainly on gradients of the gravitation potential and the matrix potential. With the seepage water, the reaction products of pyrite decomposition are transported away from the reaction front into deeper layers. A global overview of movement and behaviour of gas, water and dissolved species in the unsaturated zone is given by Hanks (1992), Lichtner and others (1996), Richter (1987), Schnoor (1996) and Wild (1993). Different models and model conceptions for pyrite decomposition in the saturated and/or unsaturated zone of overburden material are described in the literature (Davis and Ritchie 1986; Gerke and others 1998; Prein 1994; Wunderly and others 1996; Xu and others 2000). The variety of described models shows that because of the very different scenarios, frequently, new models are developed. For the modelling of the experiments presented here, the model DiffMod7 (Hecht and others 2002) was used. It considers the most important primary pyrite-decomposition processes with special consideration of the changes in oxygen concentrations over time and depth. This permits the exact comparison of the model results with the oxygen measurements made in the column experiments.

For the characterisation of the seepage water formed during pyrite decomposition geochemical modelling can be used. Some models described above are combined transport reaction models, which contain geochemical calculations to a certain extent. A second possibility is to separate modelling of the geochemical processes for example, with a thermodynamic equilibrium model such as PhreeqC (Parkhurst 1995), from the transport part.

Because the availability of oxygen is of major importance for the process of pyrite decomposition, accurate oxygen measurements are crucial. In the experiments described here, these measurements were executed with optodes, which enable temporally and spatially high-resolution measurements without influencing the concentrations during measurement (Holst 1994; Hecht and Kölling 2001a, 2001b).

One aim of this paper is to evaluate which of the processes associated with pyrite weathering may be identified and/or quantified on the basis of optical oxygen measurements. A focus is put on the identification of the active zone of pyrite decomposition and the release reactions taking place in this zone, which control the composition of the seepage water downstream. It should be clarified whether this composition can be prognosticated on the basis of the oxygen measurements and which additional parameters are important for the forecast. The aim is a worst-case estimation and forecast of the distribution and the composition of the seepage water affected by pyrite decomposition from field measurements of the ground-air oxygen distribution.

Methods and materials

Soil column experiments

Column experiments on pyrite weathering in the unsaturated zone were performed. Figure 1 shows the experimental set up. The columns were constructed from Perspex tubes with a length of 1 m and a diameter of 10 cm. The tubes were equipped with a frit at the lower end, which holds the pyrite-bearing overburden material (thickness 87 cm) over a sampling chamber. The upper end of the column is open to the atmosphere to allow gas exchange. The column was equipped with sampling ports (Luer-Lock stop cocks), which can be used for oxygen measurements with optodes. The seepage water is sampled in the chamber at the bottom of the column.

The overburden material used in the experiment for pyrite decomposition in the unsaturated zone originates from the lignite open mine Garzweiler, Germany (Neurather Sand 6D). The column was irrigated once a day and the effluent was sampled once a week. The average sample quantity was approximately 36 ml/day. The infiltration quantity (average 2,475 mm/year) was chosen to be significantly higher than natural infiltration in order to avoid a continuous situation where the depyritisation velocity

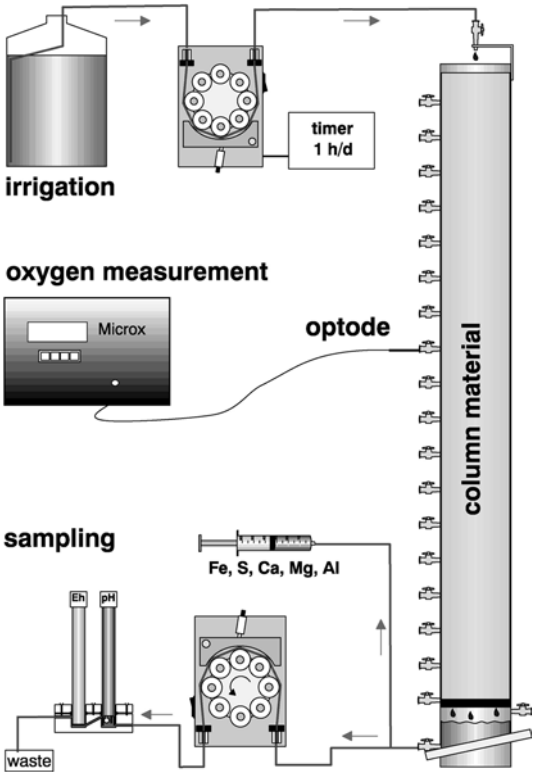

Fig. 1
Experimental set up (modified after Hecht 1998)

is higher than the seepage water velocity because this is a special small-scale effect. In natural systems this situation is found only very close to the surface. The interaction between the release of pyrite-weathering products and oxygen consumption is not affected by these experimental conditions. The total duration of the experiment was 800 days. The pH and Eh values in the effluent were monitored and the concentrations of Fe, S, Na, K, Ca, Mg and Al were determined by measurement with an ICP-AES (Perkin Elmer, Optima 3000). The oxygen measurements were performed at different temporal intervals (6 h–7 days) at depth resolutions from 10 to 2.5 cm.

Characterisation of soil column material

The material used in the column experiment was characterised before and after the experiment. The pyrite content (pyrite–sulfur content) of the overburden material was determined by chromium extraction (Volkov and Zhabina 1977). Total solid concentrations of Na, K, Ca, Mg, Al and Fe were determined by microwave digestion with hydrofluoric acid (Zabel and others 2001) and subsequent analysis of the digestion solution using an ICP-AES (Perkin Elmer, Optima 3000). After the experiments, the column was opened and the water content was determined gravimetrically in 5-cm intervals in order to obtain the porosity depth distribution. A grain size analysis of the material was executed by dry sieving.

Optical oxygen measurement

The optical oxygen measurement is based on the fluorescence-quenching effect of oxygen (Stern and Vollmer 1919). Modulated blue light is fed into an optical fibre with an oxygen-sensitive fluorescence dye applied to its tip. The fluorescence light is returned by the optical fibre and detected in the measuring instrument. In the presence of oxygen, fluorescence is quenched. Both the intensity of red fluorescence and the lifetime of fluorescence (measured as phase shift compared with the modulated blue excitation light) are dependent on oxygen concentration (Holst and others 1995). For the measurements, the optical oxygen measuring system PreSens MICROX 1 (http://www.presens.de) was used. It analyses the oxygen concentration on the basis of the fluorescence lifetime. The micro-optodes (Klimant and others 1997) used for oxygen measurement in the column experiments were adapted to use with Luer-Lock stopcocks.

Results

Characterisation of soil column material

The results of the material characterisation are shown in Table 1. The pyrite content at the beginning of the experiment is equal at all depths of the column and amounts to 1.2 wt%. The grain size analysis shows that the material is a silty (to clayey) fine sand (AG Boden 1996). The solid concentrations of Fe have decreased during the experiment at all depths. In the lower area of the column, the decrease is small and the concentrations are still close to the initial ones. The lowest iron content is found in the middle of the column. The solid concentrations of calcium also decreased. The smallest decrease in Ca was found in the upper area of the column. The changes in the solid concentrations of aluminium, magnesium, sodium and potassium are very small.

The initial total porosity of the column filling was 0.44. Because of increased irrigation, both the water content and the infiltration rate in the experiment are higher than the in-situ values of the material. Figure 2 shows the depth distribution of the air-filled porosity (effective porosity for the diffusive transport of oxygen in the gaseous phase). In the upper 60 cm of the column, values of around 0.2 are found. In the upper 10 cm, the air-filled pore space is somewhat higher by evaporation. In the lower 27 cm of the column, the water content increases. The air-filled porosity decreases to values between 0.15 and 0.08.

Release with effluent and development of oxygen concentrations

Figure 3 shows the development of pH and Eh in the effluent over time. After a short initial phase, the pH value

Table 1
Characterisation of column material

Initial pyrite content (all depths; wt%)	1.2					
Total porosity (n)	0.44					
Grain size distribution (AG Boden 1996)						
Grain size (mm)	<0.063	0.063–0.2	0.2–0.63	0.63–1	>1	
Amount (%)	24.5	60.0	13.5	1.3	0.7	
Initial solid concentrations (mol/kg)						
Element	Fe	Ca	Al	Mg	Na	K
Conc.	0.187	0.044	0.993	0.075	0.027	0.288
Final solid concentrations (mol/kg)						
Column depth (cm)	Fe	Ca	Al	Mg	Na	K
2.5	0.132	0.029	1.010	0.078	0.026	0.267
12.5	0.131	0.015	1.085	0.081	0.029	0.292
22.5	0.116	0.013	0.981	0.073	0.026	0.272
42.5	0.105	0.012	0.988	0.069	0.027	0.285
62.5	0.129	0.012	1.050	0.075	0.025	0.281
82.5	0.170	0.014	1.000	0.070	0.029	0.271

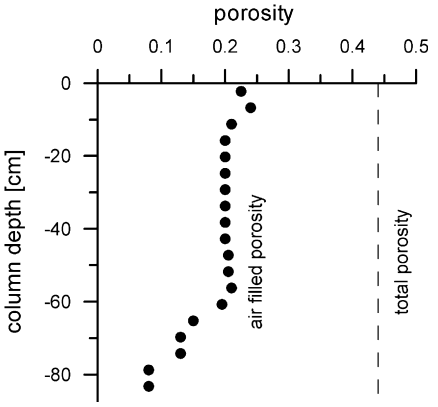

Fig. 2
Distribution of air-filled porosity over depth

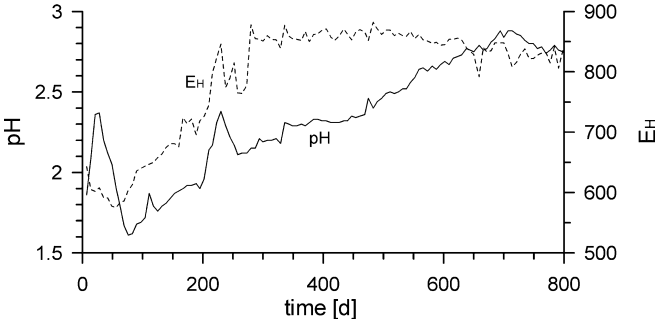

Fig. 3
Effluent pH and Eh over time

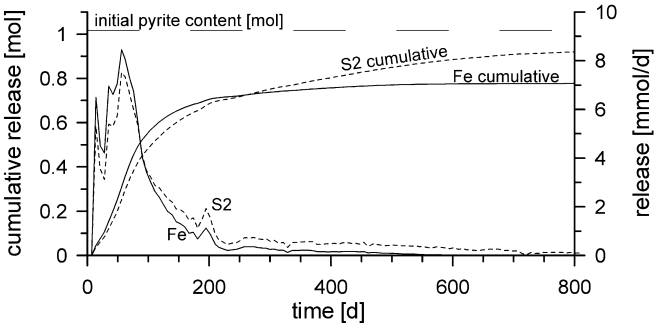

Fig. 4
Fe and S release (daily and cumulative plot); initial pyrite content

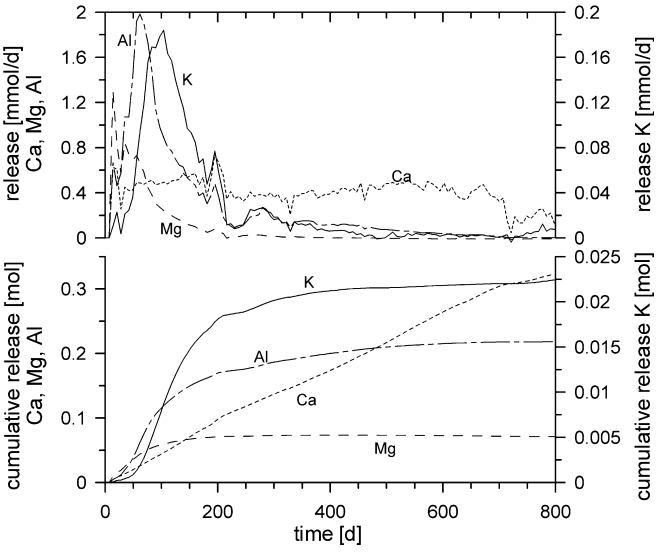

Fig. 5
Ca, Mg, Al and K release (*bottom* cumulative plot; *top* daily)

decreases to values of around 1.7 followed by a slow increase. At the beginning of the experiment, the Eh decreases, indicating that the environment in the effluent becomes more reducing. The minimum is achieved after approximately 50 days. Subsequently, the Eh continuously increases and the environment becomes more oxic. After approximately 215 days the Eh rises to values above 770 mV. A plateau value of 800 to 850 mV is found for the rest of the experiment.

The release of iron and sulfur from the column is shown in Fig. 4. Sulfur is represented as S_2 regarding the stoichiometry of pyrite. Additionally, the total initial pyrite content of the column is indicated. The graph shows both the cumulative release over time and the release per day over time. Because the effluent volumes vary, release (concentration × sample quantity) is plotted rather than concentrations. Figure 5 shows the release of calcium, magnesium, aluminium and potassium from the column. Figure 6 shows the development of oxygen concentrations within the upper 60 cm of the column over time. After column filling, oxygen is present over the whole depths with normal atmosphere partial pressure. This oxygen is quickly consumed and an equilibrium between oxygen consumption and oxygen recharge through the upper surface evolves, resulting in a decrease of oxygen ground-air concentration with depth. The oxygen concentrations at a certain depth then increase with time in the course of the experiment, indicating that oxygen penetrates more and more into the column pore space. After approximately 190 days, the oxygen concentrations show a sharp increase at all depths. Subsequently, the concentrations only increase slowly.

Distribution of pyrite

After finishing the experiment, the pyrite content was measured in different depths of the column. Figure 7 shows that the upper part of the column is pyrite-free. Below 65 cm, the pyrite content increases with depth to values of >80% of the initial pyrite content.

Discussion

Chemistry of effluent

The release of iron and sulfur with the effluent reflects the main processes within the column. At the beginning of the experiment there is a strong release of both iron and sulfur for about 80 days. This release reflects the phase of max-

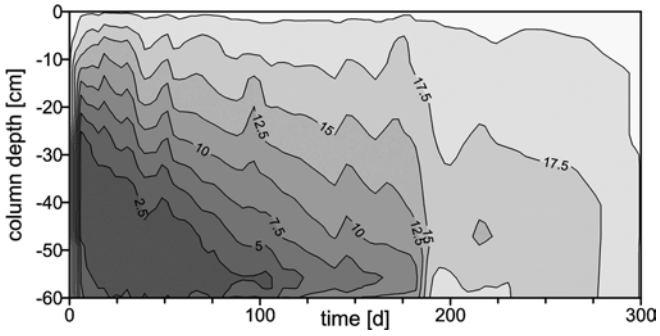

Fig. 6
Measured time–depth distribution of oxygen concentration (%) in ground air (upper 60 cm of soil column, period: 1–300th day)

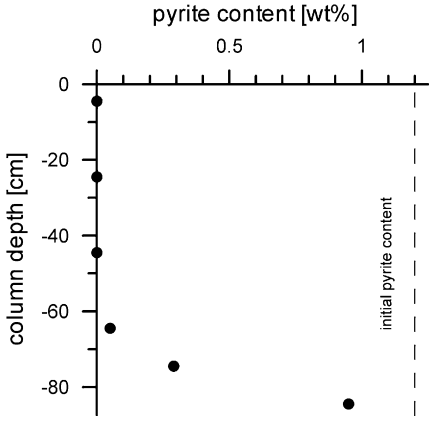

Fig. 7
Final pyrite distribution (wt%)

imum pyrite decomposition. After this period, the release decreases slowly, indicating that the total turnover of pyrite within the column decreases. After approximately 200 days, the pyrite decomposition rate strongly decreases as indicated by the decrease in iron release. At this time there is still pyrite remaining in the column as indicated by the difference in the cumulative release and the initial pyrite content. This is caused by a high water saturation of the pores in the lower part of the column as indicated by the determination of the effective pore volume. This part of the column is not ideally unsaturated resulting in an increased fraction of separated gas bubbles rather than connected pore space. In this situation, the oxygen recharge is obstructed, resulting in strongly decreased pyrite decomposition rates. The distribution of the pyrite content at the end of the experiment (see Fig. 7) reflects this fact. In the upper ideally unsaturated part of the column, the pyrite was completely dissolved. In the non-ideally unsaturated lower part of the column, the pyrite decomposition progresses very slowly. Small turnover rates result in a low but long-lasting release of the reaction products iron and sulfur.

Iron and sulfur are released by the primary process of pyrite decomposition at a constant molar ratio of 0.5 whereas the export of iron and sulfate with the effluent differs from this expected value. In the first phase of the experiment, the release of sulfate is lower than expected from the iron release. The reason is the formation of gypsum within the first 190 experiment days (see below; see Fig. 8). Subsequently, gypsum is slowly dissolved again, and sulfate is released and exported with the seepage water; thus, the sulfur release exceeds iron release. After pyrite decomposition in the ideally unsaturated area of the column is completed (after approx. 200 days) there is an additional low, but constant release of sulfur. This is a result of both gypsum dissolution and the residual pyrite decomposition in the almost saturated lower part of the column. The graph of the cumulative sulfur release slowly approaches the amount that matches the initial pyrite content of the material. The corresponding graph for iron does not show an increase after 200 days, indicating that the iron released by the pyrite decomposition process is not exported, but remains in the experimental column. Calculations with PhreeqC (Parkhurst 1995) showed that, for the first 200 days, the effluent is strongly undersaturated with respect to schwertmannite whereas, subsequently, the saturation index (SI) of schwertmannite strongly increases within a short time and approaches a SI of between –5 and 0. The strong variations within the saturation index refer to a precipitation process. Although there is a strong variability in the thermodynamic data for schwertmannite (Yu and others 1999) changes in the saturation index are significant regardless of its absolute value. The data used for the thermodynamic calculation originate from Bigham and others (1996).

The temporal changes in the pH and Eh values of the effluent also reflect the processes inside the column. The column material has a low initial buffering capacity (see below) that strongly decreases with time. The pH values decrease slowly. The lowest values are achieved after 80 days when the buffer capacity of the material is exhausted. Subsequently, the pH values slowly rise again because the total pyrite turnover in the column slowly decreases. The Eh values indicate similar processes. At the beginning of the experiment, the Eh values are stable despite decreasing pH values, showing that the environment becomes more reducing. After approximately 80 days, the Eh starts to increase slowly, although the pH increases as well, indicating that the environment is becoming more oxic. After approximately 200 days, a strong rise in Eh to values above the standard potential of the ferrous to ferric iron conversion (770 mV) shows the end of the pyrite decomposition within the ideally unsaturated area of the column. The low pH values entail different buffering reactions and dissolution/precipitation reactions, which affect the development of the pH values and strongly affect the release characteristics. Figure 8 shows the interaction of the most important processes. The fact that the release of protons does not stoichiometrically match the iron and sulfur release shows that buffer reactions must be considered. At the beginning of the experiment this is mainly the dissolution of calcite. An over saturation of gypsum and a relatively small proton release displays this process. The calcium release cannot reflect the calcite dissolution

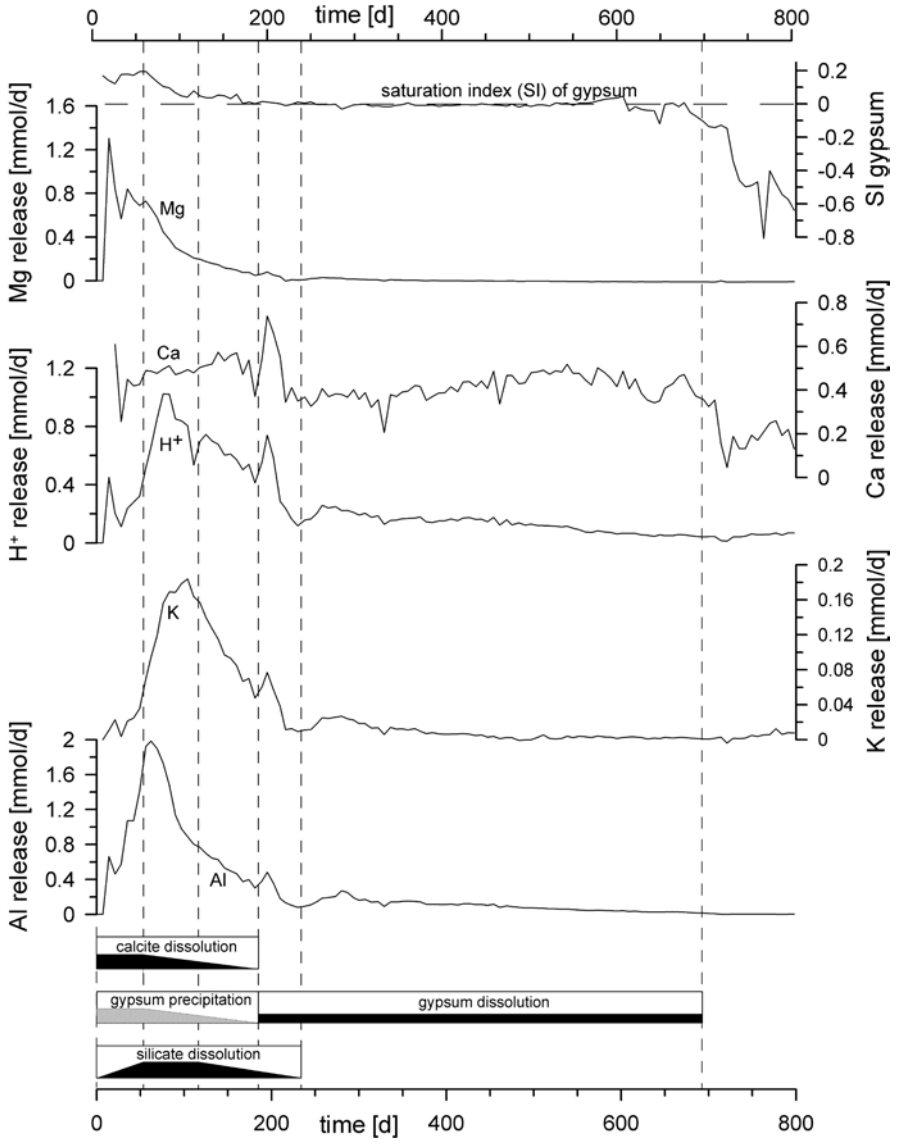

Fig. 8
Buffering and gypsum dissolution/precipitation

because most calcium is directly fixed by the precipitation of gypsum. The calcite dissolution, however, is accompanied by some magnesium release, which is not affected by secondary reactions. After 60 days, both the magnesium release and the gypsum over saturation decrease, and the proton release starts to increase indicating a strong decrease in calcite buffering. The end of residual calcite dissolution is achieved after approximately 190 days. No more calcium is released and the gypsum saturation index decreases to values of around zero, indicating that gypsum is subsequently dissolved. The export of calcium with the effluent is controlled by gypsum equilibrium until the gypsum is exhausted after approximately 690 days. After this point in time, the calcium release drops and gypsum becomes strongly undersaturated.

The release of both potassium and aluminium are primarily controlled by silicate dissolution, which is closely related to pH conditions. At the acid conditions found in the experiment, the silicate dissolution increases with decreasing pH. Figure 9 shows the correlation between pH

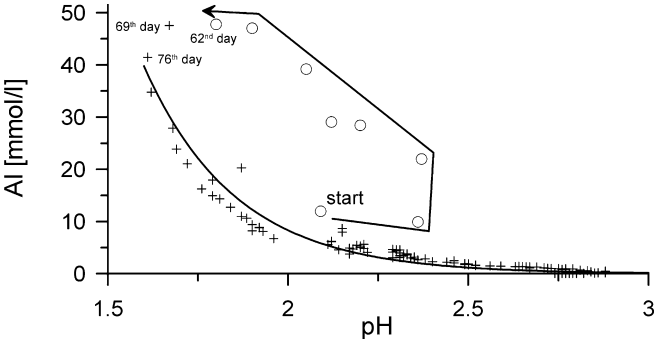

Fig. 9
Al release vs. pH

values and aluminium concentrations. From the 76th day onwards there is an exponential correlation ($a_{Al}=K\times e^{-n\times pH}$; $K=5.63\times10^5$, $n=3.91$) with an r^2 of 0.91. Within the first 60 to 70 days, additional aluminium is released from another process. This may be explained by the complete

dissolution of a limited amount of an aluminium phase, with high solubility temporarily increasing the aluminium concentration by 20 to 30 mmol/l. Calculations with PhreeqC did not reveal a possible mineral phase responsible for the additional Al-release. After the 76th day Al is only released into the seepage water by silicate dissolution. Potassium shows a good correlation with pH values throughout the experiment, which is an indication of continuous silicate dissolution.

In the aerobic pyrite oxidation process catalysed by *Thiobacillus ferrooxidans*, 1 mol of protons is released per mol of pyrite following Eq. (1) (see Introduction). The reaction includes the re-oxidation of ferrous to ferric iron in an oxic environment. If these solutions containing high amounts of ferric iron enter the anoxic part of the column, 16 mol of protons are released per mol of pyrite dissolved, accompanied with the reduction of 14 mol of ferric iron [Eq. (2)]. These conditions are met in the lower part of the experimental column throughout the experiment. Pyrite is always present and the water is anoxic as shown by the oxygen measurements. The sum reaction of reactions (1) and (2) describes the microbiologically mediated oxic decomposition of pyrite followed by an anoxic decomposition of pyrite by ferric iron. It results in Eq. (3), which is formally identical to the direct decomposition of pyrite with oxygen (Lawson 1982):

$$FeS_2 + 7/2O_2 + H_2O \rightarrow Fe^{2+} + 2SO_4^{2-} + 2H^+ \quad (3)$$

In the effluent of the experimental column, 2 mol of protons are expected per mol of pyrite dissolved. It may be shown by thermodynamic calculations with PhreeqC that, under the extreme geochemical conditions in the effluent, significant amounts of protons are subject to both complexation and buffer reactions, resulting in a pH increase. Figure 10 shows the proton balance for the duration of the entire experiment. In this graph, the cumulative release of protons (calculated from pH values and sample quantities), iron and sulfate are plotted. Only 10% of the exported protons are reflected by the pH value. PhreeqC calculations show that 15% of the protons are exported as different complexes (mainly iron and sulfate complexes). The remaining 75% of the protons are buffered in different dissolution reactions. Forty per cent of the protons are buffered by carbonate dissolution and exported as either H_2CO_3 or carbon dioxide and water. Measurable indicators of carbonate dissolution are the release of both calcium and magnesium. The remaining 35% of protons released by pyrite oxidation are buffered by either silicate dissolution or ion-exchange reactions. Measurable indicators of these processes are the release of both aluminium and potassium. Large amounts of these protons are stored in exchange sites and may act as a source for long-lasting acid release. Summing up all possible processes, the expected stoichiometric relation of 1 mol of protons per mol of sulfate released by pyrite oxidation [Eq. (3)] is only slightly exceeded at the end of the experiment. The main dissolution and buffering reactions occur within the first 200 days of the experiment whereas release of the reaction products persists over a much longer period because of secondary reactions (gypsum precipitation and dissolution).

Development of oxygen concentrations

The development of oxygen concentrations over time reflects many of the processes taking place in the column, too. The gradients in oxygen concentration show that within the column oxygen is consumed. The area in which this consumption takes place proceeds downwards throughout the experiment. At the beginning of the experiment, an equilibrium between oxygen consumption and diffusive oxygen recharge is quickly established. The fact that oxygen gradients become flatter with time indicates that the zone of oxygen consumption is displaced to greater depths, causing the oxygen flux and the pyrite decomposition to decrease slowly. This temporal change in oxygen distribution is caused by progressive depyritisation, allowing the oxygen to penetrate deeper into the column. The decrease in pyrite dissolution rates is reflected by the decrease in the release of both iron and sulfate. The effects show a time-lag of approx. 30 days, which corresponds to the seepage water velocity from the reaction location to the lower column end. After 190 days, the oxygen concentrations strongly increase at all depths of the column (see Fig. 6). This indicates a strong decrease in oxygen consumption in the column. The oxygen concentration does not reach ambient concentration, indicating that there is a small residual pyrite oxidation that persists in the lower part of the column. However, the flat

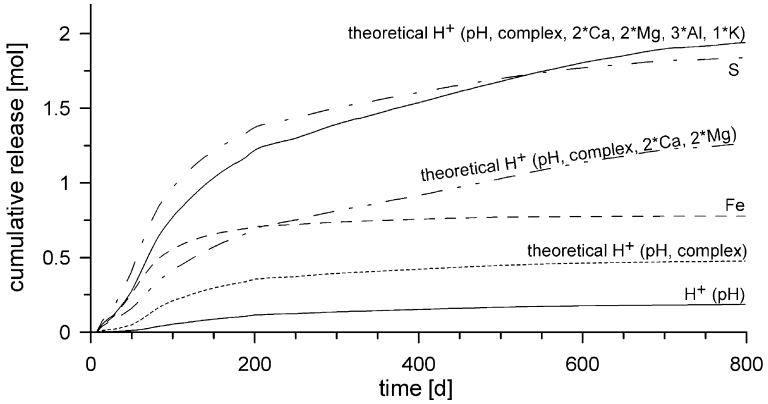

Fig. 10
Proton balance – cumulative plot

oxygen gradients show that the oxidation rate is much smaller than in the preceding stages of the experiment. Because oxygen diffusion is slow in the lower part of the column, the pyrite decomposition is slow and the temporal changes in the oxygen distribution are small (see Fig. 7). The determination of pyrite content after the experiment reveals that significant amounts of pyrite are still present in the lower part of the experimental system, supporting the assumption of residual slow pyrite oxidation in this area.

Modelling the temporal change in oxygen depth distribution

The changing intensity of pyrite decomposition can be identified from both the measured oxygen distribution and the release of reaction products. The end of pyrite decomposition within the ideally unsaturated area of the column is indicated by the change in oxygen depth distribution and by the increase in redox potential of the seepage water. In order to allow a quantitative prediction of the release of reaction products from the pyrite decomposition, the system of interest was modelled using DiffMod7 (Hecht and others 2002).

The modelling of the column experiment for pyrite decomposition is based on boundary conditions (pyrite content, porosity) determined in preliminary investigations. The tortuosity is calculated from the diffusion-effective, air-filled porosity after Boudreau (1997). Additionally, the specific pyrite surface and pyrite oxidation rate have to be provided for the model. Kölling (1990) determined a specific surface-dependent rate of 5×10^{-9} mol m^{-2} s^{-1} for pyrite decomposition catalysed by *Thiobacillus ferrooxidans* under fully oxic conditions. Values for the grain size of diagenetically formed pyrite within the overburden material used in our experiments were taken from Friedrich and others (1999). Considering some grain roughness, a good estimate for the specific surface of the pyrite is 0.5 m^2 g^{-1}. The development of oxygen concentrations modelled with DiffMod7 is shown in Fig. 11. It corresponds well with the measured oxygen depth-distributions in the column experiment.

Figure 12 compares the cumulative iron release and the pH value development in the effluent from the experiment

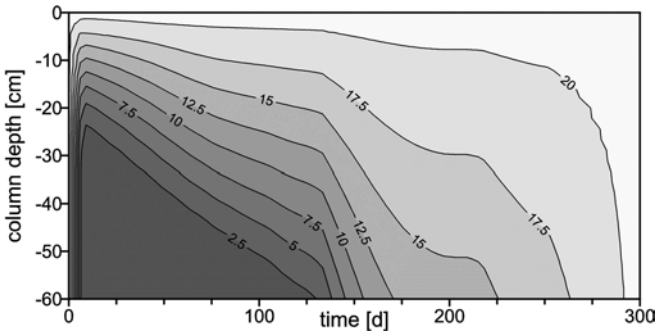

Fig. 11
Modelled time–depth distribution of oxygen concentrations (%) in ground air (modified after Hecht and others 2002)

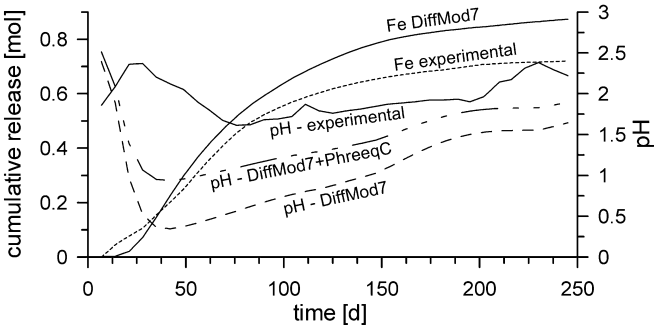

Fig. 12
Fe release and pH over time; experimental versus modelled data

and from modelling. The modelled iron release (Fe-DiffMod7) corresponds well with the data determined in the experiment. The deviations are caused by the fact that in the column experiment a part of the released iron in the column is bound by secondary reactions (see Chemistry of effluent). This plot shows that on the basis of the oxygen measurements a quite good quantification of the released amount of iron can be made. The modelled pH values (pH-DiffMod7) show significant deviations from the measured ones.

In a separate step, the results of the modelling with DiffMod7 were used as an input to PhreeqC in order to calculate a more realistic pH considering all complexation equilibria. This calculation generally results in higher pH values, which are also plotted in Fig. 12 (pH-Diffmod7-PhreeqC). The remaining differences between measured and modelled pH values are because no buffering reactions are considered in DiffMod7. The pH values resulting from the model with subsequent PhreeqC calculation may be seen as a worst-case approximation of pH values for material without acid-buffering capacity. The residual difference in pH can be used to quantify the amount of protons buffered by dissolution reactions.

Further results that can be derived from the modelling with DiffMod7 are the time–depth distributions of pyrite turnover, pyrite content and the seepage water concentration (see Fig 13). The plot of modelled pyrite turnover (Fig. 13, left) shows the formation of an initial pyrite decomposition zone in the upper 30 cm of the column. Within this area, pyrite decomposition occurs at maximum rates because of non-obstructed oxygen recharge. With progressing depyritisation (Fig. 13, centre) the oxygen penetrates deeper into the column. A narrow zone evolves at which all oxygen is consumed by pyrite weathering. Both the width of the front and the pyrite turnover in the front become smaller as the surface distance of the front location increases (Hecht and others 2002). At the end of the modelled scenario, the column is pyrite-free throughout the total length (60 cm). The distribution of seepage water constituents (Fe, S) indicates that the maximum concentrations occur in the water that was at the upper edge of the pyrite decomposition zone at the beginning of the experiment.

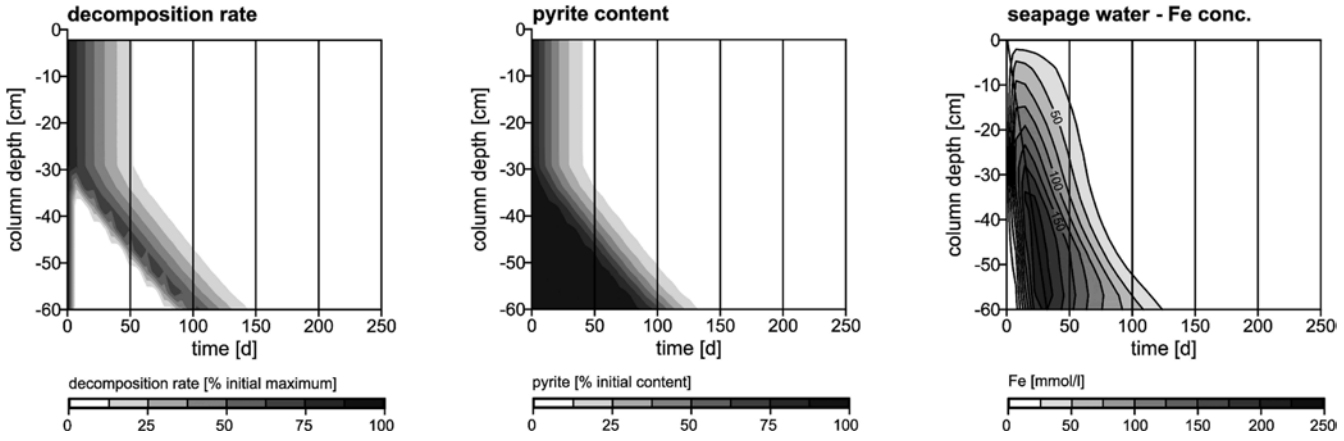

Fig. 13
Modelled decomposition rate, pyrite content and seepage water Fe conc. (modified after Hecht and others 2002)

In an oxygen-consuming system, different information may be derived from oxygen measurements and modelling as shown above. In a field test at a 43-year-old dump body, both the measuring system and the model could be used to reveal that there is still pyrite oxidation going on at a depth of approximately 6 m (Hecht and others 2002).

Conclusions

The total potential for acidification is determined by the initial pyrite content of overburden material stored above groundwater level. For the primary release and subsequent distribution of the reaction products, further factors are crucial. The oxygen recharge is the most important factor controlling the primary pyrite decomposition process. It limits the thickness of the layer in which pyrite decomposition occurs and is responsible for the total amount of pyrite decomposition. In the column experiment presented, the overburden material with a pyrite content of 1.2 wt% was completely depyritised within 200 days down to a depth of 0.6 m. The rate decreases exponentially. Oxygen measurements inform us about the status of the system. The actual location of the pyrite decomposition front and, thus, the depyritisation depth can be determined. If, additionally, the initial pyrite content and diffusion-effective porosity are known, the actual release of decomposition products and the remaining acidification potential can be determined. The temporal development of the systems can be simulated by modelling the data. A prognosis for the release and distribution of iron and sulfur is possible. The buffer capacity of the system and the seepage water velocity are crucial for the distribution of reaction products. In the experiment presented, 75% of the released protons were consumed by reactions with calcite and silicate. Fifteen per cent of the protons were fixed to complexes and delivered with the effluent. Although only 10% of the protons are represented by the measured pH value, seepage water with pH values below pH 2 develops. For a correct prognosis of the pH value in such systems it is essential to quantify the buffer capacity and to consider buffering reactions in the geochemical part of the model.

Acknowledgements This work was carried out in the Section of Geochemistry and Hydrogeology headed by Prof. H.D. Schulz, Department of Geosciences, University of Bremen. The project was supported by a grant from the Deutsche Forschungs Gemeinschaft (DFG-Ko-1656/2-1). This paper represents publication no. 177 of the Priority Program 546 "Geochemical processes with long-term effects in anthropogenically affected seepage water and groundwater".

References

AG Boden (1996) Bodenkundliche Kartieranleitung. 4. Aufl., Nachdr, Hannover

Appelo CAJ, Postma D (1994) Geochemistry, groundwater and pollution. Balkema, Rotterdam

Bigham JM, Schwertmann U, Traina SJ, Winland RL, Wolf M (1996) Schwertmannite and the chemical modeling of iron in acid sulfate waters. Geochim Cosmochim Acta 60:2111–2121

Boudreau BP (1997) Diagenetic models and their implementation – modelling transport and reactions in aquatic sediments. Springer, Berlin, Heidelberg New York

Davis GB, Ritchie AIM (1986) A model of oxidation in pyritic mine wastes. 1. Equations and approximate solution. Appl Math Modell 10:314–322

Evangelou VP (1995) Pyrite oxidation and its control. CRC Press, Boca Raton

Friedrich G, Dohrmann R, Jochum J, Echle W, Wiechowski A, Lang R, Riebeiro-Rodrigues LC (1999) Mineralinhalt und Spurenelementverteilung im Neurather Sand – Ihre Bedeutung für die Freisetzung umweltrelevanter Metalle beim Braunkohleabbau im Niederrheinischen Revier. Z Angew Geol 45(1):37–48

Gerke HH, Molson JW, Frind EO (1998) Modelling the effect of chemical heterogeneity on acidification and solute leaching in overburden mine spoils. J Hydrol 209:166–185

Hanks RJ (1992) Applied soil physics – soil water and temperature applications. Springer, Berlin Heidelberg New York

Hecht H (1998) Optodenmessung zur Bestimmung diffusiver Sauerstoffnachlieferung bei der Pyritverwitterung. Diploma Thesis, Department of Geosciences, University of Bremen

Hecht H, Kölling M (2001a) A very low attenuation fiber optical sensor switch (LAFOSS). Sensors Actuators B 81(1):128–131

Hecht H, Kölling M (2001b) A low-cost optode-array measuring system based on 1 mm plastic optical fibers – new technique for

in-situ detection and quantification of pyrite weathering processes. Sensors Actuators B 81(1):76–82
Hecht H, Kölling M, Geissler N (2002) DiffMod7 – modelling oxygen diffusion and pyrite decomposition in the unsaturated zone based on ground air oxygen distribution. In: Geochemical processes – concepts for modelling reactive transport in soils and groundwater. Wiley-VCH, Weinheim (in press)
Holst G (1994) Entwicklung und Erprobung einer Sauerstoff-Flux-Optode mit einem Sauerstoff-Sensor nach dem Prinzip der dynamischen Fluoreszenzlöschung. Fortschrittberichte VDI, Reihe 17: Biotechnik 111. VDI Verlag, Düsseldorf
Holst G, Kühl M, Klimant I (1995) A novel measuring system for oxygen micro-optodes based on a phase modulation technique. Proc SPIE 2508–45:387–398
Klimant I, Kühl M, Glud RN, Holst G (1997) Optical measurement of oxygen and temperature in microscale: strategies and biological applications. Sensors Actuators B 38–39:29–37
Kölling M (1990) Modellierung geochemischer Prozesse im Sickerwasser und Grundwasser – Beispiel: Die Pyritverwitterung und das Problem saurer Grubenwässer. Ber FB Geowiss Univ Bremen 8
Lawson RT (1982) Aqueous oxidation of pyrite by molecular oxygen. Chem Rev 82:461–497
Lichtner PC, Steefel CI, Oelkers EH (eds) (1996) Reactive transport in porous media. Mineral Soc Am, Washington, DC
Mattheß G (1991) Lehrbuch der Hydrogeologie – Band 2: Die Beschaffenheit des Grundwassers. Gebr Borntraeger Berlin
Nordstrom DK (1982) Aqueous pyrite oxidation and the consequent formation of secondary iron minerals. In: Kittrick JA, Fanning DF, Hossner LR (eds) Acid sulfate weathering: pedogeochemistry and relationship to manipulation of soil materials. Soil Science Society of America, pp 37–56
Parkhurst DL (1995) User's guide to PHREEQC – a computer program for speciation, reaction-path, advective-transport, and inverse geochemical calculations. WRIR 95-4227, US Geological Survey
Prein A (1994) Sauerstoffzufuhr als limitierender Faktor für die Pyritverwitterung in Abraumkippen von Braunkohletagebauen. Mitteilungen, Institut für Wasserwirtschaft, Hydrologie und Landwirtschaftlichen Wasserbau der Universität Hannover 79
Richter J (1987) The soil as a reactor – modelling processes in soil. Catena, Cremlingen
Schnoor LJ (1996) Environmental modelling: fate and transport of pollutants in water, air, and soil. Wiley, New York
Stern O, Volmer M (1919) Über die Abklingzeit von Fluoreszenz. Physikalische Z 20:183–188
Volkov II, Zhabina NN (1977) Determination of pyritic sulfur with metallic chromium and chromium (II) solution. In: Ostroumov EA (ed) Chemical analysis of marine sediments. Nauka, Moscow, pp 5–14
Wild A (1993) Soils and the environment – an introduction. Cambridge University Press, Cambridge
Wunderly MD, Blowes DW, Frind EO, Ptacek CJ (1996) Sulfide mineral oxidation and subsequent reactive transport of oxidation products in mine tailings impoundments: a numerical model. Water Resour Res 32:3173–3187
Xu T, White SP, Preuss K, Brimhall GH (2000) Modelling of pyrite oxidation in saturated and unsaturated subsurface flow systems. Transport Porous Media 39:25–56
Yu J-Y, Heo B, Choi I-K, Cho J-P, Chang H-W (1999) Apparent solubilities of schwertmannite and ferrihydrite in natural stream waters polluted by mine drainage. Geochim Cosmochim Acta 63(19/20):3407–3416
Zabel M, Schneider RR, Wagner T, Adegbie A, de Vries U, Kolonic S (2001) Late Quaternary climate changes in central Africa as inferred from terrigenous input to the Niger Fan. Quat Res 56:207–217